Jurnal
Teknologi

Full Paper

INVESTIGATION OF GAS PERMEABILITY IN PET/GRAPHENE NANOCOMPOSITES FOR FOOD PACKAGING APPLICATIONS

Mohd Ihsan Che Mohd Noh, Mohd Ambri Mohamed, Azrul Azlan Hamzah, Abang Annuar Ehsan*, A. Atiqah

Institute of Microengineering and Nanoelectronics (IMEN), Universiti Kebangsaan Malaysia (UKM), 43000 Bangi, Malaysia

Article history
Received
23 June 2025
Received in revised form
8 December 2025
Accepted
18 December 2025
Published Online
29 Augustr 2026

* Corresponding author
aaehsan@ukm.edu.my
r

Graphical abstract

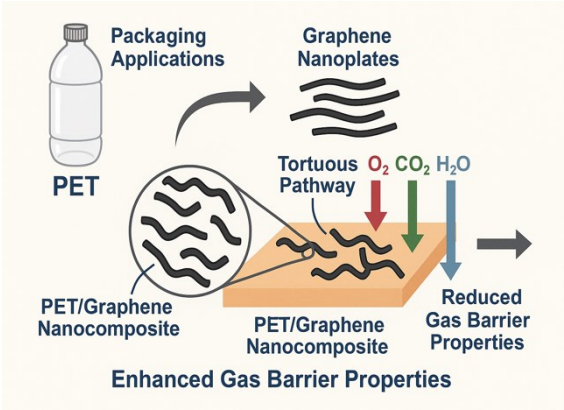

Abstract

Polyethylene terephthalate (PET) is widely used in packaging applications due to its excellent mechanical and thermal properties. However, its intrinsic gas permeability limits its performance in high-barrier applications. The incorporation of graphene-based nanofillers into the PET matrix has emerged as a promising strategy to significantly enhance gas barrier properties. In this study, the gas permeability behavior of PET/graphene nanocomposites was investigated using a 3D-structured graphene nanoplatelet (GNP) network designed to maximize tortuosity within the polymer matrix. The addition of graphene nanoplatelets introduces a highly tortuous three-dimensional diffusion pathway that impedes the transport of gas molecules, thereby markedly containing 0.3 wt% graphene nanoplatelets. This improvement correlates with microstructural changes evidenced by BET analysis, where the specific surface area increased from 0.53 m^2/g for neat PET to 1.18 m^2/g for the 0.3 wt% GNP composite, and the total pore volume increased from 4.33×10^{-4} cm^3/g to 1.07×10^{-3} cm^3/g, reflecting the development of a more complex 3D internal pathway. The degree of barrier enhancement was strongly dependent on dispersion quality, graphene loading, aspect ratio, and interfacial interaction between the filler and polymer matrix. This combination of low graphene content, quantified barrier improvement, and a tailored 3D tortuous network showed the novelty of this work and highlights the potential of PET/graphene nanocomposites for advanced packaging, electronics encapsulation, and functional barrier applications.

Keywords: PET Graphene; Nanocomposite; Gas permeability; Barrier properties; Oxygen transmission rate (OTR)

Abstrak

Polietilena tereftalat (PET) digunakan secara meluas dalam aplikasi pembungkusan kerana sifat mekanikal dan terma yang sangat baik. Namun, kebolehtelapan gas intrinsiknya mengehadkan prestasi dalam aplikasi penghalang tinggi. Penggabungan nanopensel graphene ke dalam matriks PET telah muncul sebagai strategi yang berpotensi untuk meningkatkan sifat penghalang gas dengan ketara. Dalam kajian ini, tingkah laku kebolehtelapan gas bagi nanokomposit PET/graphene telah dikaji dengan menggunakan rangkaian nanoplatelet graphene (GNP) berstruktur 3D yang direka untuk memaksimumkan kesukaran laluan (tortuosity) dalam matriks polimer. Penambahan nanoplatelet

graphene memperkenalkan laluan penyebaran tiga dimensi yang sangat berliku, yang menghalang pergerakan molekul gas, sekali gus memberikan pengekangan yang ketara pada kepekatan 0.3 wt% nanoplatelet graphene. Peningkatan ini berkaitan dengan perubahan mikrostruktur yang dibuktikan melalui analisis BET, di mana luas permukaan khusus meningkat daripada 0.53 m^2/g bagi PET tulen kepada 1.18 m^2/g bagi komposit GNP 0.3 wt%, dan jumlah isipadu liang meningkat daripada 4.33×10^{-4} cm^3/g kepada 1.07×10^{-3} cm^3/g, mencerminkan pembangunan laluan dalaman 3D yang lebih kompleks. Tahap peningkatan penghalang sangat bergantung pada kualiti serakan, kandungan graphene, nisbah aspek, dan interaksi antara muka antara pengisi dan matriks polimer. Gabungan kandungan graphene yang rendah, peningkatan penghalang yang terukur, dan rangkaian tortuosity 3D yang direka bentuk ini menunjukkan keaslian kajian ini serta menonjolkan potensi nanokomposit PET/graphene untuk aplikasi pembungkusan termaju, enkapsulasi elektronik, dan aplikasi penghalang berfungsi.

Kata kunci: PET Graphene; Nanokomposit; Kebolehtelapan gas; Sifat penghalang; Kadar transmisi oksigen (OTR)

1.0 INTRODUCTION

Polyethylene terephthalate (PET) is a widely used thermoplastic polymer known for its excellent mechanical strength, chemical resistance, and transparency. However, its inherent gas permeability limits its application in fields requiring high barrier performance, such as food packaging and electronics encapsulation [1], [2]. To overcome this limitation, researchers have explored the development of nanocomposites by incorporating various nanofillers into the PET matrix. Among these, graphene and its derivatives have attracted significant attention due to their exceptional mechanical, thermal, and impermeable properties.

Graphene, with its atomically thin two-dimensional structure and high aspect ratio, serves as an effective barrier against gas diffusion when dispersed within a polymer matrix. The incorporation of graphene nanosheets into PET creates a tortuous path for gas molecules, effectively reducing the rate at which gases such as oxygen permeate through the material [3]. This phenomenon, often described by the tortuous path model, results in a significant reduction of the oxygen transmission rate (OTR), enhancing the overall barrier properties of the composite. Even at low graphene loadings, substantial improvements in gas barrier performance have been observed, making PET/graphene nanocomposites a promising solution for applications where extended shelf life and product protection are critical [4], [5].

The performance of PET/graphene nanocomposites depends on several factors, including the dispersion quality of graphene within the PET matrix, the aspect ratio of graphene nanosheets, and the interfacial adhesion between the filler and the polymer. Proper functionalization of graphene can further enhance its compatibility with PET, leading to better dispersion and more effective barrier properties [6], [7]. As research advances, the optimization of processing techniques and filler characteristics continues to open new possibilities for utilizing PET/graphene nanocomposites in high-performance barrier applications.

Research over the past decade consistently shows that adding a very small fraction of graphene or its derivatives to PET films produces a pronounced drop in gas transport. Early demonstrations with graphene oxide (GO) sheets dispersed in PET cut oxygen transmission by roughly two-thirds at 1 wt. % loading, confirming the tortuous-path concept proposed for other platelet fillers [8]. Subsequent work extended the concept to reduced GO and exfoliated graphite nanoplatelets (EGNPs), reporting comparable 60–70 % reductions in both O_2 and CO_2 flux at similar loadings [9], [10]. Collectively, these studies established that high-aspect-ratio graphene sheets, even at sub-percent concentrations, are markedly more effective barriers than traditional clays or talc because their atomic-scale thickness maximises aspect-ratio-to-volume fraction, lengthening the diffusion path far more efficiently.

In another works done by Ashfaq *et al*. [10] demonstrated that dropping from 1 wt % to just 0.5 wt % GNPs still delivered an 82 % reduction in oxygen permeability, indicating that most of the barrier enhancement arises once a partial labyrinth of platelets spans the polymer matrix. Zhao *et al*. [11] showed a ~70 % fall in water-vapour permeability at 0.4 wt. % GNPs, but only marginal extra gain when the filler was doubled. These results are attributed to the onset of platelet restacking and micro-void formation at higher viscosities, which counteract the intended barrier effect.

Recent advances in the field have shifted focus from merely quantifying permeability to optimizing

processing techniques that enhance graphene dispersion and orientation within polymer matrices. For example, melt compounding with in-situ compatibilizers [12] and twin-screw extrusion followed by solid-state drawing [13] have both been shown to significantly improve the alignment of graphene platelets. This improved alignment results in an additional 10–15% reduction in gas permeability compared to samples with unaligned fillers at equivalent loadings, underscoring the importance of processing conditions in achieving superior barrier properties. Building upon these established methods, our study introduces a novel approach by transforming the well-dispersed PET/graphene composite pellets into filaments suitable for fused-filament 3D printing. This innovative step allows for the direct fabrication of food-packaging prototypes, leveraging the advantages of additive manufacturing. Not only does this method maintain the enhanced barrier properties achieved during compounding, but it also enables the creation of customized container geometries and supports rapid, on-demand production. To the best our knowledge, very few or less attempt on PET–graphene nanocomposite filaments being utilized in 3D-printed food packaging applications. This approach bridges the gap between advanced material development and practical manufacturing, offering a versatile platform for producing high-barrier packaging solutions tailored to specific requirements capabilities that have not yet been documented in the existing PET–graphene packaging literature.

2.0 METHODOLOGY

2.1 Materials

Commercial-grade PET filament served as the polymer matrix, while high-purity graphene nanoplatelets (GNPs) acted as the reinforcement to boost the thermal and mechanical performance of wall panels. A ball-milling step was adopted to disperse the GNPs uniformly throughout the PET, promoting strong interfacial bonding. The resulting PET/GNP blend was pelletised and fed to a filament extruder, producing composite feedstock that was subsequently shaped into test specimens via 3D printing.

2.2 Preparation of PET Graphene Nanocomposites

PET and graphene were combined via a carefully controlled planetary-ball-milling route. A stainless-steel jar and balls were selected to eliminate any risk of contamination while achieving the fine, uniform particle size that this mill affords. Prior to milling, PET filament was cut into small chips, then blended with graphene flakes at three loadings 0.1 wt %, 0.3 wt %, and 0.5 wt % to study the influence of graphene content on the final material. The blend was milled for 4 h at 350 rpm using a 10 : 1 ball-to-powder mass ratio, supplying sufficient impact energy to reduce particle size and yield a well-mixed PET/graphene powder.

2.2 Sample fabrication of PET Graphene Nanocomposites

The extrusion process is a key manufacturing technique used in the fabrication of PET-graphene composites, which combines polyethylene terephthalate (PET) with GNPs to enhance material properties. In this process, the PET-graphene composite is heated to a specific temperature range of 185-190 °C, allowing the polymer matrix to soften and become moldable. Once the material reaches this molten state, it is forced through a die to produce a filament with a uniform diameter of 1.75 mm, suitable for subsequent applications such as 3D printing. The precise control of temperature during the extrusion process is critical to ensure the proper dispersion of graphene within the PET matrix, which directly influences the composite's mechanical, thermal, and barrier properties.

Figure 1 shows the extruder machine used to produce PET-GNPs composite filament. In this process, the PET-GNPs mixture is fed into the extruder, where it is subjected to controlled heating and mechanical shearing. As the material moves through the heated barrel, it melts and becomes thoroughly mixed, ensuring that the graphene is evenly dispersed within the PET matrix. The molten composite is then forced through a die to form a continuous filament, which is subsequently cooled and collected for further processing or testing. The use of an extruder is essential for achieving consistent filament diameter and uniform material properties, both of which are critical for applications such as 3D printing and advanced manufacturing.

Figure 1 The extrusion process of PET-GNPs filament using mechanical extruder machine

The PET-GNPs composite filaments with 0.1%, 0.3%, and 0.5% graphene concentrations were successfully used to 3D print dog bone and square shapes using a Creality printer machine, as shown in Figure 2. The 3D printing process was carried out at a nozzle temperature of 220 °C and a bed temperature of 90 °C, ensuring optimal adhesion and print quality. Dog bone specimens were printed for subsequent tensile testing to evaluate the mechanical strength of each composition, while square-shaped samples were produced for gas permeability testing to assess the barrier properties of the composite. These tests will provide insights into how the varying graphene concentrations affect gas barrier performance of the PET-GNPs composites.

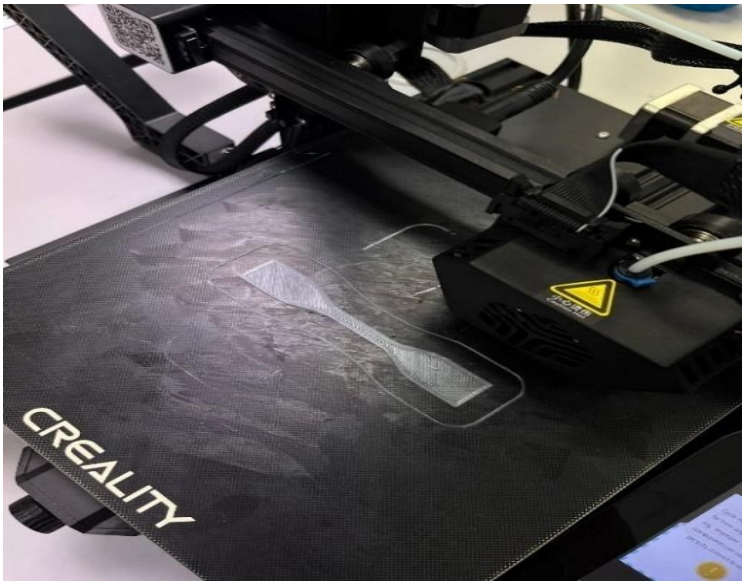

Figure 2 Creality 3D-printer machine used to 3D print dog bone and square shape for tensile test and gas permeability characterization

3.0 CHARACTERIZATION

Prior to characterization, the samples were dried and finely ground to ensure homogeneity and improve surface accessibility during analysis. Approximately 0.1–1.0 g of each sample was used for testing. To eliminate residual moisture and volatile impurities, the samples were degassed under vacuum at elevated temperatures at 60 °C for 3 hours, depending on their thermal stability.

The gas permeability and barrier performance of the PET–GNP nanocomposites were indirectly evaluated based on their porosity and pore size distribution using the Brunauer–Emmett–Teller (BET) method. Nanocomposite films with varying graphene nanoplatelet (GNP) concentrations (0, 0.1, 0.3, and 0.5 wt%) were prepared, ground when necessary, and subjected to nitrogen adsorption–desorption analysis at 77 K using a BET surface area analyzer Micromeritics ASAP 2020. From the nitrogen adsorption–desorption isotherms, the BET specific surface area, total pore volume, and average pore diameter were determined. These parameters were used to assess microstructural changes and to correlate the development of a more tortuous internal pathway with the expected improvements in gas barrier performance of the PET–GNP nanocomposites.

The microstructure and fracture morphology of neat PET and PET/graphene nanocomposites were examined by scanning electron microscopy (SEM). Film specimens were cryo-fractured in liquid nitrogen to expose representative cross-sections, and the fractured surfaces were sputter-coated with a thin conductive gold or gold–palladium layer to minimize charging during imaging. SEM observations were carried out at an accelerating voltage in the range of 5–20 kV. The SEM images were used to evaluate the dispersion state of the graphene nanoplatelets, identify possible agglomerates, and characterize the fracture behavior (brittle versus ductile features, surface roughness, and presence of microvoids). Special attention was given to the morphology of the optimized 0.3 wt% GNP nanocomposite, enabling a direct link between the observed three-dimensional tortuous microstructure and the BET-derived porosity metrics, as well as the enhanced gas barrier performance.

4.0 RESULT AND DISCUSSION

4.1 Morphology Properties of PET-GNPs Nanocomposite

SEM images of the surface as shown in Figure 3 show a morphology of PET and PET-Graphene at variation concentration (a) PET, (b) PET – 0.1% C, (c) PET – 0.3% C and (d) PET – 0.5% C. Figure 3 (a) SEM micrograph of PET shows a homogeneous, compact, and predominantly brittle fracture surface, with a rough, lamellar texture, isolated small pits, and no clearly visible secondary phases or large cracks at the observed scale. For Figure 3 (b) The PET – 0.1% C sample shows a compact, homogeneous, brittle fracture surface that looks very similar in character to neat PET, with only minor additional small pits or defects. There is no visual evidence of strong GNP agglomeration or large filler-related defects in this field of view; the morphology suggests that at this low loading, the GNP does not drastically alter the large-scale fracture appearance of the PET matrix. While for Figure 3 (c), the fracture surface is brittle, rough, and compact, with a continuous PET matrix and no macroscopic cracks or porous channels. There are more localized pits and small cavity-like defects than in neat PET, likely reflecting increased internal heterogeneity and interfaces at this loading. However, no large, discrete GNP agglomerates are visible at this magnification, the filler phase is not directly resolved as distinct platelets in this Figure 3 (c). The SEM image of PET containing 0.5 wt% graphene nanoplatelets as in Figure 3 (d) reveals a rough and predominantly brittle fracture surface. The matrix remains generally compact and continuous, with no large through-thickness cracks or macrovoids visible at this magnification. However, the surface exhibits a greater number of small pits and cavity-like features relative to neat PET and lower filler loadings (Figures 3 (b) – (c), suggesting increased microstructural heterogeneity associated with filler–matrix interfaces. No large, discrete graphene agglomerates are clearly resolved in this field of view, indicating that, at the micrometer scale of observation, the filler is not present as massive clusters, although sub-micrometer aggregates cannot be excluded.

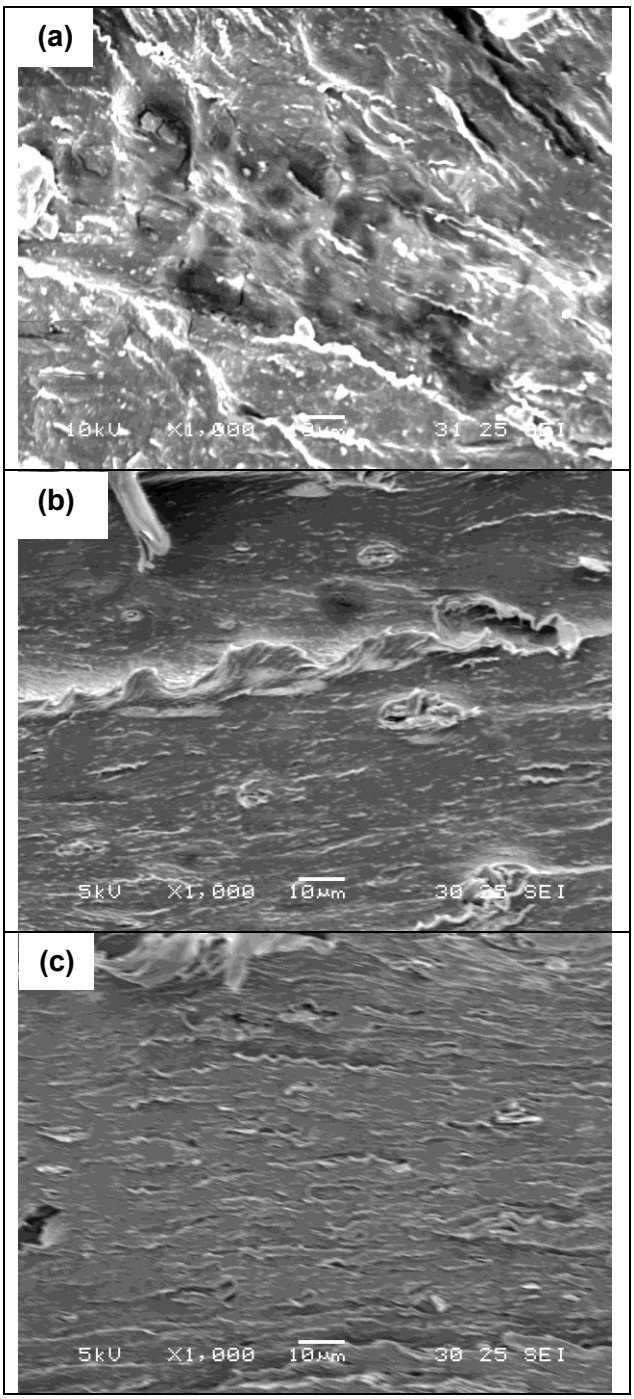

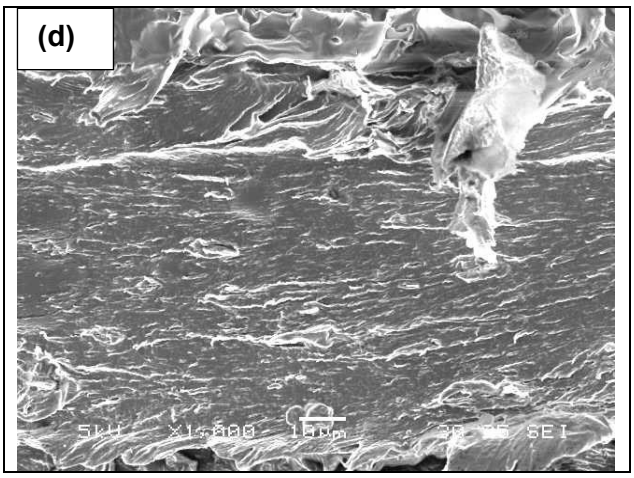

Figure 3 Morphology of PET and PET-Graphene at variation concentration (a) PET, (b) PET – 0.1% C, (c) PET – 0.3% C and (d) PET – 0.5% C

4.2 Evaluation of Gas Barrier Properties of PET-GNPs Nanocomposite

The (Brunauer-Emmett-Teller) BET gas permeability test is a technique used to measure the specific surface area, pore volume, and pore size distribution of PET and PET reinforced with graphene by analyzing the adsorption of nitrogen gas molecules on the surface of a sample. Based on Table 1, the BET surface area increases significantly when carbon content is increased to 0.3% C, reaching 1.1820 m²/g. However, at 0.5% C, the BET surface area decreases to 0.9273 m²/g. This suggests that the addition of carbon initially promotes the formation of more surface area but further increases in carbon concentration led to a slight reduction in surface area, possibly due to aggregation or blocking of pores as discussed in Section 4.1 in Figure 1(d).

Table 1 Comparison of surface area and porosity parameters for PET and PET/Carbon blend

Sample	BET Surface Area (m^2/g)	Total Pore Volume (cm^2/g)	Average Pore Size (nm)
PET	0.5275	0.000433	3.7859
PET – 0.1% C	0.3983	0.000326	4.3527
PET – 0.3% C	1.1820	0.001074	4.3655
PET – 0.5% C	0.9273	0.000765	4.3751

The total pore volume follows a similar trend to the surface area. PET-0.3% C shows a significant increase in pore volume, indicating a more porous structure. PET-0.5% C sees a decrease in total pore volume compared to PET-0.3% C, which could imply that the pores are being filled or blocked as the carbon content increases further.

The average pore size increases gradually with the addition of carbon. This indicates that carbon incorporation leads to larger pore sizes, which could be beneficial for applications requiring larger channels for diffusion or adsorption. Therefore, the addition of carbon to PET significantly impacts its surface area, pore volume, and pore size. The optimal increase in BET surface area and total pore volume occurs at 0.3% C, beyond which both parameters decrease slightly. The average pore size, however, increases steadily with the addition of more carbon.

4.3 Pore size distribution of PET-GNPs Nanocomposites

The analysis of pore size distribution in PET and PET reinforced with graphene provides valuable insights into the structural modifications imparted by graphene incorporation. Figure 4 demonstrates PET without any reinforcement shows a standard pore size distribution primarily in the range of 1-10 nm. The pore size distribution is relatively narrow, indicating a uniform structure with limited porosity. This can be attributed to the dense packing of polymer chains, pronounced peak in the 20-50 nm range. This substantial increase in pore size can be attributed to which results in fewer voids and small-sized pores. The presence of these small pores typically affects the material's overall mechanical properties, potentially leading to lower toughness and impact resistance.

Upon reinforcing PET with graphene, significant changes in pore size distribution are observed. Introducing 0.1% graphene into PET begins to alter the pore size distribution. The presence of graphene nanoparticles increases the number of pores in the 5-20 nm range. This suggests that even a small amount of graphene can start modifying the porosity and potentially enhancing certain material properties.

The inclusion of graphene, particularly at low concentrations, results in a wider distribution of pore sizes. With 0.3% graphene, there is a more significant shift in pore size distribution. Most pores now appear in the 10-30 nm range. This indicates that graphene at this concentration is effectively creating larger interstitial spaces within the PET matrix, potentially leading to improved mechanical and thermal properties. This suggests that graphene acts as a nucleating agent, creating more pores and larger voids within the PET matrix. These larger pores can enhance the composite's toughness by providing sites for energy dissipation during deformation, thereby improving fracture toughness.

At higher concentrations of graphene, the pore size distribution shows a further increase in the number and size of pores. At 0.5% graphene reinforcement, the pore size distribution shows the higher loading of graphene, which disrupts the polymer matrix more significantly, resulting in larger

pores. This can enhance gas permeability and other functional properties but may also affect the material's structural integrity if not managed properly.

This phenomenon is likely due to the agglomeration of graphene particles, which can create significant voids within the composite structure. These voids can act as stress concentrations, potentially reducing the material's strength but enhancing its toughness and energy absorption capabilities. The balance between these opposing effects determines the overall mechanical performance of the composite.

The structural changes observed in the pore size distribution due to graphene reinforcement also impact the thermal and electrical properties of the composite. Larger pores and a more interconnected porous structure can facilitate better thermal conductivity by providing pathways for heat transfer. Similarly, the electrical conductivity of the composite can be enhanced due to the formation of conductive networks within the porous structure, especially if the graphene is well-dispersed. The research done by Noh showed that adding 2 wt% of GNP to PET reduced gas permeation by about 99%. SEM analysis indicated the formation of micropores in the PET/GNP nanocomposite, which contributed to the improved gas barrier properties [14]. Study done by Al-Bustami discovered that PET nanocomposites containing graphite nanoplatelets were prepared by melt compounding. These nanocomposites exhibited superior oxygen barrier properties and improved thermal and dimensional stability compared to plain PET films. For 1.5 wt% GNP, oxygen permeation was reduced by more than 99%, attributed to the exfoliated morphology and good mixing with PET [4].

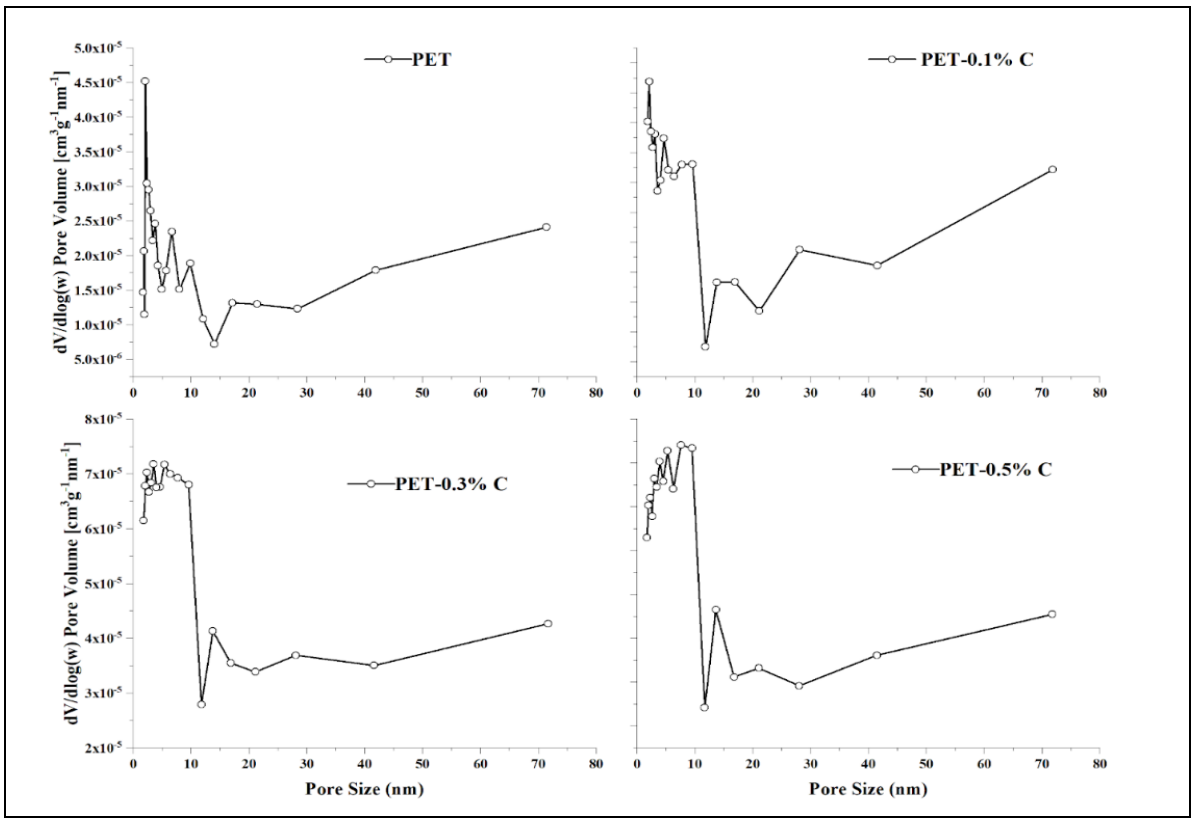

Figure 4 Pore size distributions of PET and PET-Graphene at variation concentration

4.4 Pore Volume Distribution of PET-GNPs Nanocomposites

In the case of pure PET, the BET analysis in Figure 5 shows a small pore volume of 0.000433 cm³/g and a pore width of 3.7859 nm. This suggests a compact structure with limited porosity, which is characteristic of pure PET due to its tight molecular arrangement. The low pore volume aligns with the relatively small surface area of 0.5275 m²/g, indicating minimal porosity. This structure is typical for polymers like PET that have not been modified with additives, limiting their gas permeability and surface reactivity.

When carbon is added at 0.1%, the pore width increases significantly to 4.3527 nm, but the total pore volume decreases to 0.000326 cm³/g. This inverse relationship between pore width and pore volume suggests that the increased pore size may be the result of fewer but larger pores, which could indicate that carbon particles are creating wider channels within the PET matrix but not necessarily increasing the overall number of pores. Such behavior has been

observed in other studies where small amounts of carbon additives lead to structural rearrangements, resulting in larger, fewer pores rather than a higher number of smaller pores.

At 0.3% carbon concentration, the pore volume increases significantly to 0.001074 cm³/g, while the pore width increases slightly to 4.3655 nm. The increased pore volume combined with the larger pore width indicates that the carbon is now contributing to both an increase in the number and size of the pores. This suggests enhanced porosity, which is consistent with findings from other research on carbon-modified polymers. For instance, similar increases in pore volume and pore size have been reported when carbon is incorporated into polymer matrices, promoting the formation of a more porous structure that could improve gas permeability and adsorption properties.

In the PET-0.5% C sample, the pore width continues to increase slightly to 4.3751 nm, while the pore volume decreases to 0.000765 cm³/g. This again suggests an inverse relationship between pore width and pore volume. The slight reduction in pore volume may be due to the aggregation of carbon particles at higher concentrations, which can block or fill some of the pores, resulting in a decrease in total pore volume even as the average pore size remains large. Other studies on carbon composites have shown that higher concentrations of carbon can lead to pore blockage, reducing the overall porosity despite larger pore sizes.

Research comparing the effects of carbon incorporation on pore structure has shown similar trends. Studies on carbon-doped polymeric materials have found that pore width generally increases with carbon incorporation, but beyond an optimal level, the pore volume can decrease due to pore blocking effects [11]. Similarly, in activated carbon fibers, researchers observed that while pore width can increase with higher carbon loading, there is often a reduction in pore volume, attributed to agglomeration or the collapse of pore structures at higher carbon percentages [15]. These trends are consistent with our analysis of the PET samples. The optimal balance between pore width and pore volume is observed at moderate carbon concentrations (e.g., 0.3% C), beyond which the structural integrity of the pores can be compromised by excessive carbon, leading to a reduction in available pore volume. In conclusion, carbon incorporation affects both the pore width and volume in PET samples. The optimal carbon content for maximizing pore volume without excessive reduction in pore size appears to be around 0.3% C. Beyond this concentration, the pore structure becomes less favorable for gas adsorption due to pore blocking or aggregation effects. These findings align with broader research on carbon-doped materials.

4.5 Langmuir Surface Area Distribution of PET-GNPs Nanocomposites

In the Langmuir surface area plot based on Figure 6, the relationship between pressure and p/Q for the PET sample is expected to follow a typical adsorption pattern, where p/Q decreases as pressure increases due to higher adsorption at higher pressures. Since PET without carbon incorporation has a relatively lower BET surface area, its Langmuir plot will likely show a more gradual slope. This suggests that fewer adsorption sites are available for gas molecules at lower pressures, which is consistent with its lower total pore volume.

The PET-0.1% C sample would show a slightly steeper curve in the Langmuir plot compared to pure PET. The introduction of 0.1% carbon increases the pore size, which could result in a higher initial p/Q ratio at lower pressures. However, the decrease in total pore volume implies that the sample might reach saturation earlier, showing a flattening of the curve at higher pressures. This suggests that while there are larger pores available for gas adsorption, the total number of available pores is reduced, affecting the overall adsorption capacity.

The PET-0.3% C sample is expected to show the most pronounced deviation in the Langmuir plot, as both the pore volume and BET surface area reach their maximums at this concentration. This sample would likely exhibit a steep decline in p/Q with increasing pressure, indicating a rapid adsorption process due to the higher number of available adsorption sites. The increased surface area and larger pore volume at 0.3% carbon provide more spaces for gas molecules to adhere, leading to a more efficient adsorption at lower pressures.

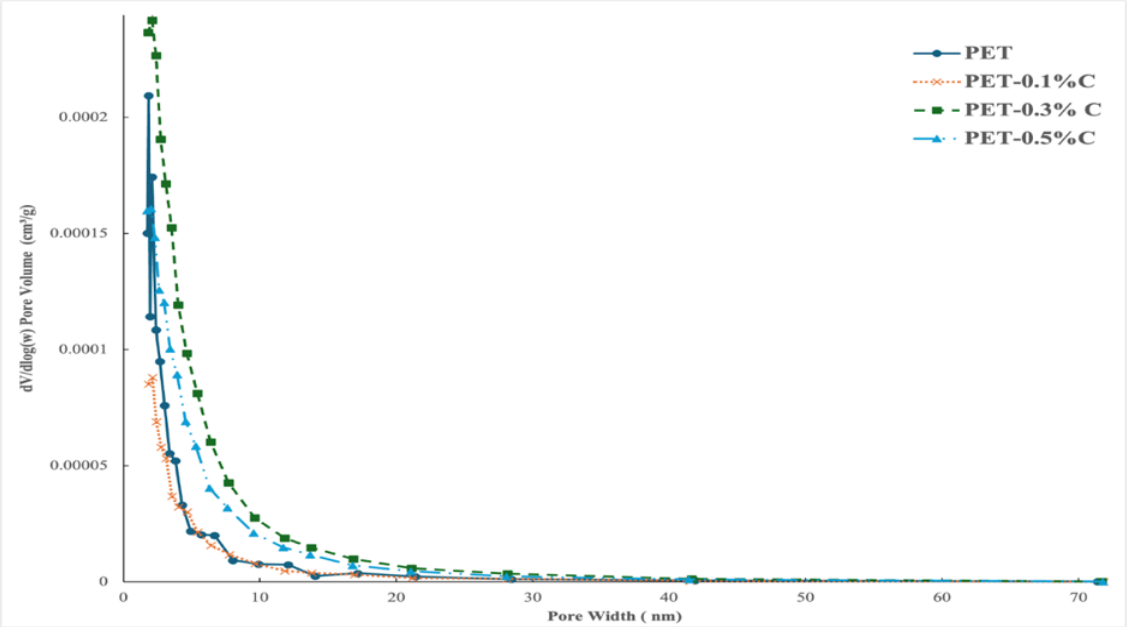

Figure 5 Pore width of the PET and PET-Graphene versus pore volume

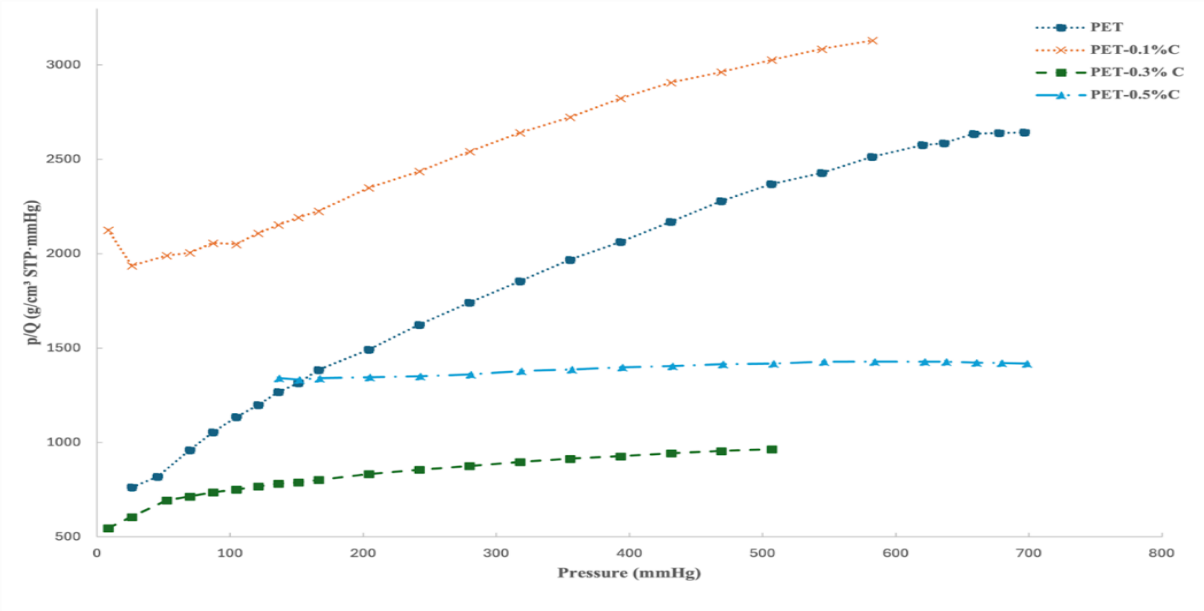

Figure 6 Langmuir surface area of PET and PET-Graphene plot at varying concentration

The PET-0.3% C sample is expected to show the most pronounced deviation in the Langmuir plot, as both the pore volume and BET surface area reach their maximums at this concentration. This sample would likely exhibit a steep decline in p/Q with increasing pressure, indicating a rapid adsorption process due to the higher number of available adsorption sites. The increased surface area and larger pore volume at 0.3% carbon provide more spaces for gas molecules to adhere, leading to a more efficient adsorption at lower pressures.

For the PET-0.5% C sample, the Langmuir plot may show a behavior similar to PET-0.1% C but with slightly more available surface area and pore volume. While the pore size increases marginally, the decrease in total pore volume indicates that at higher pressures,

the adsorption process might slow down more quickly, leading to an earlier plateau in the Langmuir curve. This is consistent with the idea that excessive carbon incorporation can block or reduce access to adsorption sites, limiting the overall adsorption capacity.

Studies on carbon-modified polymers often show that the Langmuir surface area increases with moderate carbon addition due to enhanced pore structures. Other researchers suggested that the introduction of carbon improves adsorption efficiency at lower pressures, but excessive carbon can lead to pore blockages that reduce the material's overall adsorption capacity [16], [17]. Similar observations are made in carbon-based nanomaterials, where the adsorption capacity peaks at optimal carbon loading, followed by a decline as pore blockages occur [18].

4.6 BJH Adsorption Area of PET-GNPs Nanocomposites

Figure 7 depicts the BJH Adsorption dA/dlog(w) Pore Area vs. Pore Width for PET and its carbon-doped variants of PET-0.1% C, PET-0.3% C, and PET-0.5% C. This plot helps in understanding the distribution of pore areas across different pore widths, giving insights into the material's porosity profile and its capacity for adsorption. By analyzing how the pore area changes with pore width, we can evaluate the impact of carbon incorporation on the porosity and potential applications of the material.

In the PET sample, the BJH plot shows that most of the pore area is concentrated around smaller pore widths. The distribution suggests that pure PET is characterized by micropores or small mesopores, which contribute to its overall limited surface area. The relatively narrow range of pore widths indicates that pure PET is less suitable for applications requiring a diverse range of pore sizes, such as catalysis or gas separation. The lack of significant larger pore areas limits the material's versatility in these applications.

The introduction of 0.1% carbon leads to a shift in the BJH adsorption profile, with a broader range of pore widths and an increase in the total pore area. The dA/dlog(w) value increases, indicating that carbon incorporation promotes the formation of larger mesopores, which contribute more significantly to the total surface area compared to pure PET. However, the pore area increase remains modest, suggesting that while there is an enhancement in the material's porosity, the structure may still not be ideal for high-performance adsorption applications.

The PET-0.3% C sample exhibits the most significant shift in the BJH adsorption profile. The pore area is spread across a wider range of pore widths, including both mesopores and macropores. The dA/dlog(w) curve demonstrates a marked increase in pore area for larger pores, making PET-0.3% C more suitable for applications like gas storage, filtration, and catalysis that require diverse pore sizes.

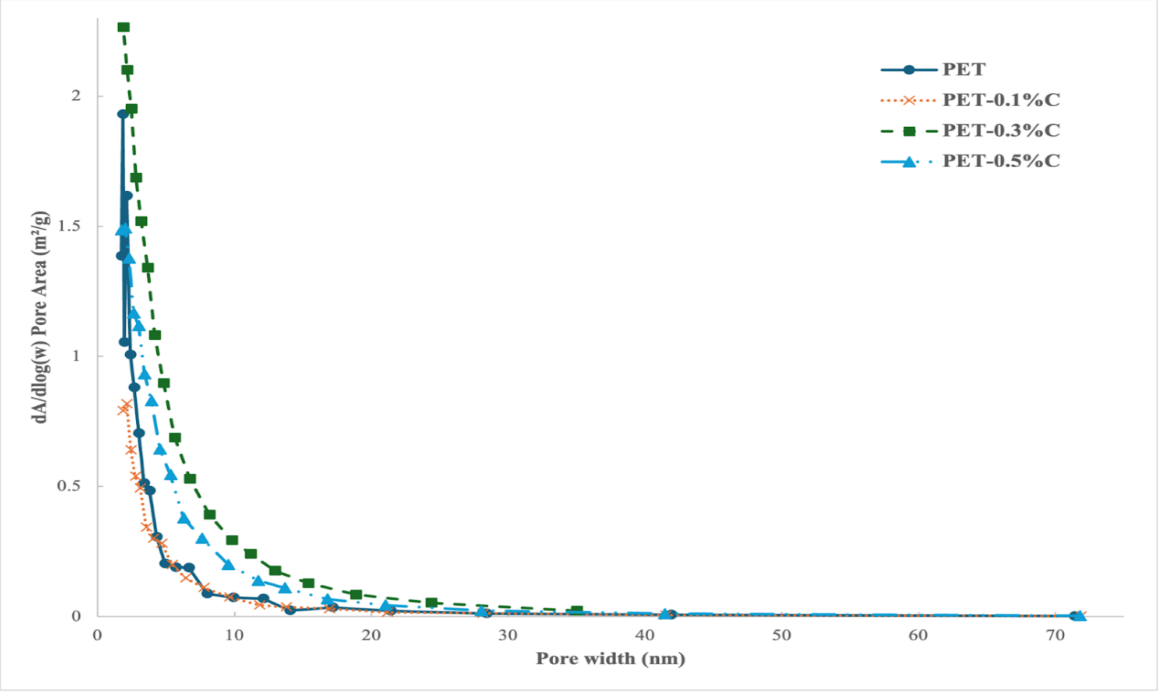

Figure 7 BJH Adsorption dA/dlog(w) Pore Area vs Pore width

This broader pore distribution reflects the material's improved porosity and enhanced adsorption capacity, making it the most effective composition for energy storage and separation processes.

At 0.5% carbon incorporation, the BJH plot shows that while the pore width continues to increase, the distribution of pore area becomes more irregular. The total pore area does not increase as significantly as seen in the PET-0.3% C sample, suggesting that pore blockage or aggregation effects may be occurring. Although the material still has a broader range of pore sizes compared to pure PET, the optimal balance between pore width and area achieved at 0.3% carbon is not maintained. This may limit its effectiveness in applications requiring large surface areas and high adsorption efficiency.

Research on carbon-modified materials typically shows that moderate carbon addition improves the porosity and pore size distribution of the material. For instance, in carbon-modified alumina, moderate carbon incorporation enhances the mesopore and macropore area, leading to improved adsorption capacity and performance in gas separation applications [19]. Similar observations have been made in carbon-doped porous polymers, where increased carbon content results in larger pore widths but can also lead to a decrease in total pore area due to pore blocking at higher concentrations [18].

Width analysis demonstrates the impact of carbon incorporation on the porosity of PET. The optimal carbon content for enhancing both pore area and width is at 0.3% carbon, which creates a broad distribution of pore sizes, improving the material's potential for adsorption and filtration applications. At higher carbon concentrations, pore blockage can reduce the total pore area, limiting the material's effectiveness in certain applications. This behavior is consistent with findings from other carbon-modified materials.

4.7 Relationship between Cumulative Surface Area of PET-GNPs Nanocomposites

Figure 8 presents the relationship between cumulative surface area (m^2/g) and pore width (nm) for PET and its carbon-doped variants: PET-0.1% C, PET-0.3% C, and PET-0.5% C. This plot helps to illustrate how pore width influences the overall surface area of the materials, which is a key factor in determining their performance in applications such as catalysis, adsorption, and filtration. By evaluating the cumulative surface area with respect to pore width, we can assess how carbon incorporation affects the porous structure of PET.

For the pure PET sample, the cumulative surface area increases steadily at smaller pore widths. Most of the surface area is contributed by smaller pores, indicating that pure PET has a microporous structure with limited mesopores. This results in a lower overall cumulative surface area, which limits its potential in applications requiring extensive surface interactions, such as adsorption and catalysis. The lack of larger pores restricts the material's versatility, as it provides For the pure PET sample, the cumulative surface area increases steadily at smaller pore widths. Most of the surface area is contributed by smaller pores, indicating that pure PET has a microporous structure with limited mesopores. This results in a lower overall cumulative surface area, which limits its potential in applications requiring extensive surface interactions, such as adsorption and catalysis. The lack of larger pores restricts the material's versatility, as it provides fewer pathways for gas or fluid flow through the structure. With the introduction of 0.1% carbon, the cumulative surface area of the PET-0.1% C sample shows a slight increase at larger pore widths compared to pure PET. This indicates that carbon incorporation helps to create some mesopores, which contribute to a higher surface area. However, the increase in surface area remains moderate, suggesting that 0.1% carbon loading does not drastically alter the porous structure of PET. The material's improved performance in adsorption applications is likely due to a marginal enhancement in pore size distribution, though it may not be sufficient for high-demand applications requiring substantial surface areas.

The PET-0.3% C sample exhibits the most significant increase in cumulative surface area across a wider range of pore widths. The plot shows that a substantial portion of the surface area is contributed by both mesopores and macropores, making PET-0.3% C an ideal candidate for applications requiring high This optimal balance is often seen in carbon-modified materials where moderate carbon content results in improved surface area and pore structure [20]. In the PET-0.5% C sample, while the cumulative surface area continues to increase with pore width, the rate of increase is less dramatic than in the PET-0.3% C sample. This suggests that although the pore width is larger, the overall surface area is not expanding as efficiently. This behavior may be due to pore blockage or aggregation effects, where the excessive carbon content reduces the accessibility of some pores. Consequently, while PET-0.5% C still has a larger cumulative surface area than pure PET, its performance may not be as effective as the PET-0.3% C sample in applications requiring a high degree of porosity and surface interaction. Similar observations have been made in studies on carbon-doped polymers, where optimal carbon loading enhances surface area, but excessive loading leads to reduced effectiveness due to pore blockage [21], [22].

The BET pore width vs. cumulative surface area analysis from Figure 8 highlights the impact of carbon incorporation on the porous structure of PET. The PET-0.3% C sample demonstrates the most favorable balance between pore width and surface area, making it suitable for high-performance adsorption, filtration, and catalysis applications. In contrast, excessive carbon incorporation in PET-0.5% C leads to diminished returns in surface area, likely due to pore

blocking. These findings are consistent with other research on carbon-doped materials, where moderate carbon content optimizes the material's porosity and surface area [20].

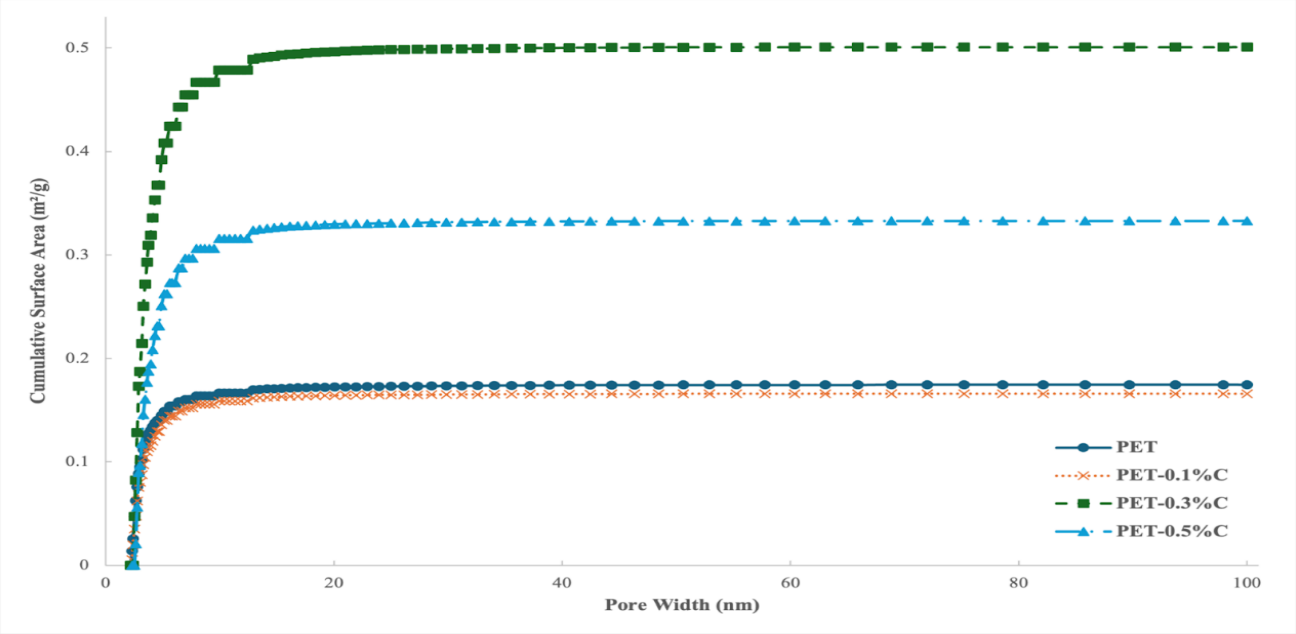

Figure 8 Cumulative Surface Area (m2/g) vs Pore Width (nm) emhancing the material's performance in applications where a balance between surface area and pores size is crucial

5.0 CONCLUSION

In this study, PET/graphene nanocomposites were successfully fabricated and their gas permeability properties were quantitatively evaluated. The incorporation of graphene into the PET matrix significantly improved the barrier properties primarily due to the tortuous path effect created by the dispersed graphene nanoplatelets. The optimized composition containing 0.3 wt% graphene nanoplatelets, From BET analysis further supported these findings: neat PET showed a specific surface area of 0.53 m^2/g and a total pore volume of 4.33 × 10^{-4} cm^3/g, whereas the 0.3 wt% graphene nanocomposite exhibited an increased surface area of 1.18 m^2/g and a pore volume of 1.07 × 10^{-3} cm^3/g, indicating significant changes in the accessible microstructure and interfacial area. Even at low graphene loadings (≤ 0.5 wt%), substantial reductions in gas permeability were observed, demonstrating the effectiveness of graphene as a functional barrier additive. The extent of improvement was strongly influenced by the dispersion quality, graphene content, and interfacial interactions between the polymer matrix and the nanofiller. These results highlight that a PET nanocomposite with 0.3 wt% graphene nanoplatelets offers an optimal balance between filler loading and barrier performance. Overall, PET/graphene nanocomposites show strong potential for advanced packaging applications where enhanced gas barrier performance is critical. Further optimization of processing techniques and graphene surface modification could yield even greater improvements in barrier efficiency, making these materials promising candidates for future high-performance packaging and functional barrier applications.

Acknowledgement

The authors would like to express their sincere gratitude to Universiti Kebangsaan Malaysia for providing the laboratory facilities and technical support required to carry out this research.

Conflicts of Interest

The authors declare that there is no conflict of interest regarding the publication of this paper.

References

[1] Usman, I. U., and Kunlin. 2024. Influence of Polyethylene Terephthalate (PET) Utilization on the Engineering Properties of Asphalt Mixtures: A Review. *Construction and Building Materials*. https://doi.org/10.1016/j.conbuildmat.2023.134439.

[2] Combeau, M., *et al*. 2023. A Comparative Study on Crystallisation for Virgin and Recycled Polyethylene Terephthalate (PET): Multiscale Effects on Physico-

Mechanical Properties. *Polymers.* 15(23): 4613. https://doi.org/10.3390/polym15234613.
[3] Kim, D., *et al.* 2021. Diamine Vapor Treatment of Viscoelastic Graphene Oxide Liquid Crystal for Gas Barrier Coating. *Scientific Reports.* 11. https://doi.org/10.1038/s41598-021-88955-5.
[4] Al-Bustami, H., A. Al-Jabareen, G. Marom, and H. Harel. 2012. Improving the Oxygen Barrier Properties of Polyethylene Terephthalate by Graphite Nanoplatelets. *Journal of Applied Polymer Science*. 128: 1534–39. https://doi.org/10.1002/app.38302.
[5] Cui, Y., S. Kumar, S. Kundalwal, and S. Kumar. 2016. Gas Barrier Performance of Graphene/Polymer Nanocomposites. *Carbon*. 98: 313–33. https://doi.org/10.1016/j.carbon.2015.11.018.
[6] Ramzan, N., S. Qamar, and W. Aleem. 2024. Graphene Dispersion, Functionalization Techniques, and Applications: A Review. *Synthetic Metals*. https://doi.org/10.1016/j.synthmet.2024.117697.
[7] Kanny, K., A. P. Rath, and S. G. Krishnan. 2023. Studies on Polyethylene Terephthalate Hybrid Polymer Nanocomposites. *Polymer Bulletin*. https://doi.org/10.1007/s00289-023-04799-1.
[8] Allahbakhsh, A. 2017. High Barrier Graphene/Polymer Nanocomposite Films. In *Graphene-Based Polymer Nanocomposites in Electronics*. Elsevier. https://doi.org/10.1016/B978-0-12-804302-8.00020-0.
[9] Saxena, D., N. Soundararajan, V. Katiyar, D. Rana, and P. Maiti. 2020. Structural, Mechanical, and Gas Barrier Properties of Poly(ethylene terephthalate) Nanohybrid Using Nanotalc. *Journal of Applied Polymer Science*. 137(27): 1–12. https://doi.org/10.1002/app.48607.
[10] Ashfaq, J., *et al*. 2023. Enhancement of Thermal and Gas Barrier Properties of Graphene-Based Nanocomposite Films. *ACS Omega.* 8(44): 41054–63. https://doi.org/10.1021/acsomega.3c02885.
[11] Zhou, M., *et al.* 2024. Mechanism of Gas Barrier Improvement of Graphene/Polypropylene Nanocomposites for New-Generation Lightweight Hydrogen Storage. *Composites Science and Technology*. 110483. https://doi.org/10.1016/j.compscitech.2024.110483.
[12] Hareesha, M., B. Yogesha, L. L. Naik, and D. Saravanabavan. 2021. Development on Graphene-Based Polymer Composite Materials and Their Applications: A Recent Review. *AIP Conference Proceedings.* 2316. https://doi.org/10.1063/5.0036854.
[13] Lawal, A. T. 2020. Recent Progress in Graphene-Based Polymer Nanocomposites. *Cogent Chemistry*. 6(1): 1833476. https://doi.org/10.1080/23312009.2020.1833476.
[14] Noh, M. I. C. M., M. A. Mohamed, A. G. Ismail, M. H. Ani, and B. Y. Majlis. 2019. Improvement of Gas Barrier Properties of Polyethylene Terephthalate (PET) by Graphene Nanoplatelets (GNP). *Materials Today: Proceedings.* 7: 808–15. https://doi.org/10.1016/j.matpr.2018.12.079.
[15] Lee, H.-M., S.-H. Kang, B.-J. Kim, and K.-W. Kim. 2021. Synthesis and Characterization of Activated Carbon Fibers Derived from Linear Low-Density Polyethylene Fibers Stabilized at a Low Temperature. *Polymers.* 13(22): 3918. https://doi.org/10.3390/polym13223918.
[16] Wang, Y., *et al*. 2023. Precise Preparation of Biomass-Based Porous Carbon with Pore Structure-Dependent VOCs Adsorption/Desorption Performance by Bacterial Pretreatment and Its Forming Process. *Environmental Pollution*. 121134. https://doi.org/10.1016/j.envpol.2023.121134.
[17] Dilokekunakul, W., P. Teerachawanwong, N. Klomkliang, S. Supasitmongkol, and S. Chaemchuen. 2020. Effects of Nitrogen and Oxygen Functional Groups and Pore Width of Activated Carbon on Carbon Dioxide Capture: Temperature Dependence. *Chemical Engineering Journal.* 389: 124413. https://doi.org/10.1016/j.cej.2020.124413.
[18] Perovic, M., Q. Qin, and M. Oschatz. 2020. From Molecular Precursors to Nanoparticles—Tailoring the Adsorption Properties of Porous Carbon Materials by Controlled Chemical Functionalization. *Advanced Functional Materials.* 30: 1908371. https://doi.org/10.1002/adfm.201908371.
[19] Chen, C., X. Ding, Y. Wang, Z. Luo, and P. Zhai. 2022. Fractal Dimension Analysis of Structure and Bending Strength of Porous Alumina Prepared Using Starch and Carbon Fiber as Pore-Forming Agents. *Fractal and Fractional.* 6(10): 574. https://doi.org/10.3390/fractalfract6100574.
[20] Deng, S., *et al*. 2020. Solving Two Environmental Issues Simultaneously: Waste Polyethylene Terephthalate Plastic Bottle-Derived Microporous Carbons for Capturing CO_2. *Chemical Engineering Journal.* 397: 125350. https://doi.org/10.1016/j.cej.2020.125350.
[21] Abu-Dief, A., *et al.* 2024. Recent Advances in Heteroatom-Doped/Hierarchically Porous Carbon Materials: Synthesis, Design, and Potential Applications. *Progress in Materials Science*. 101408. https://doi.org/10.1016/j.pmatsci.2024.101408.
[22] Zhang, M., *et al*. 2020. Polymer-Derived Heteroatom-Doped Porous Carbon Materials. *Chemical Reviews*. https://doi.org/10.1021/acs.chemrev.0c00080.